

Detectability of Microwave Background Polarization

Emory F. Bunn*

Physics Department, University of Richmond, Richmond, VA 23173

(Dated: November 5, 2018)

Measurement of the amplitudes of both the E and B components of the CMB polarization will open new windows onto the early Universe. Using a Fisher-matrix formalism, we calculate the required sensitivities and observing times for an experiment to measure the amplitudes of both E and B components as a function of sky coverage, taking full account of the fact that the two components cannot be perfectly separated in an incomplete sky map. We also present a simple approximation scheme that accounts for mixing of E and B components in computing predicted errors in the E-component power spectrum amplitude. In an experiment with small sky coverage, mixing of the two components increases the difficulty of detecting the subdominant B component by a factor of two or more in observing time; however, for larger survey sizes the effect of mixing is less pronounced. As a result, the optimal experimental setup for detecting the B component must cover an area of sky significantly larger than is found when mixing is neglected. Surprisingly, mixing of E and B components can enhance the detectability of the E component by increasing the effective number of independent modes that probe this component. The formalism presented in this paper can be used to explore ways in which survey geometry and nonuniform noise due to uneven sky coverage will affect detectability of the two components.

PACS numbers: 98.70.Vc, 98.80.Es, 98.80.Cq, 98.80.-k

I. INTRODUCTION

The cosmic microwave background radiation (CMB) contains a wealth of information about the high-redshift Universe. Efforts to map the temperature anisotropy and estimate its power spectrum have already revolutionized our understanding of cosmology, strongly suggesting that the Universe is spatially flat and constraining other cosmological parameters (*e.g.*, [1, 2, 3, 4, 5, 6, 7]). Future anisotropy measurements, especially the MAP [8] and Planck [9] satellite missions, will allow the cosmological parameters to be determined with unprecedented precision (*e.g.*, [10, 11]).

Polarization will be the next frontier in the study of the CMB; considerable effort is already underway (*e.g.*, [12, 13, 14]) to map the CMB polarization structure. That the CMB should be polarized is an extremely robust prediction [15, 16] of the gravitational instability paradigm of standard cosmological theory, so detection of CMB polarization will provide a reassuring confirmation of the standard model. Moreover, a large amount of additional information is expected to be lurking in CMB polarization maps. Measurement of the CMB polarization power spectra will help in breaking certain degeneracies between cosmological parameters [17, 18, 19, 20]. But perhaps most exciting of all is the possibility that CMB polarization measurements will contain the signature of primordial gravity waves (tensor perturbations) produced during an inflationary epoch [21, 22, 23]. If these hopes are realized, we will have far more direct evidence than we currently do that inflation actually occurred, and we will have probed the Universe at far earlier times than any current observations.

Detecting the gravity-wave signal in a CMB polarization data set will be a daunting task: the tensor contribution to the CMB polarization is expected to be considerably smaller than the contribution due to scalar density perturbations. Fortunately, the tensor contribution has a geometrically different signature from the scalar contribution, allowing the two to be separated. To be specific, any polarization map can be split into two components [21, 22]: the “E component,” which transforms as a scalar, and the “B component,” which transforms as a pseudoscalar.¹ Scalar

*Electronic address: ebunn@richmond.edu

¹ The division of a polarization field into E and B components is closely analogous to the division of a vector field into curl-free and divergence-free parts. This is the reason for naming the components after the electric and magnetic fields. (Of course it is hardly necessary to add that these names have nothing to do with the actual electric and magnetic fields of the radiation.) Elsewhere in the literature, the two components are called G and C, for “gradient” and “curl” respectively. If the world needed yet another name for these components (which it certainly doesn’t), they could be called + and ×; as we will see below, these give the orientation of the polarization with respect to the wavevector in Fourier space.

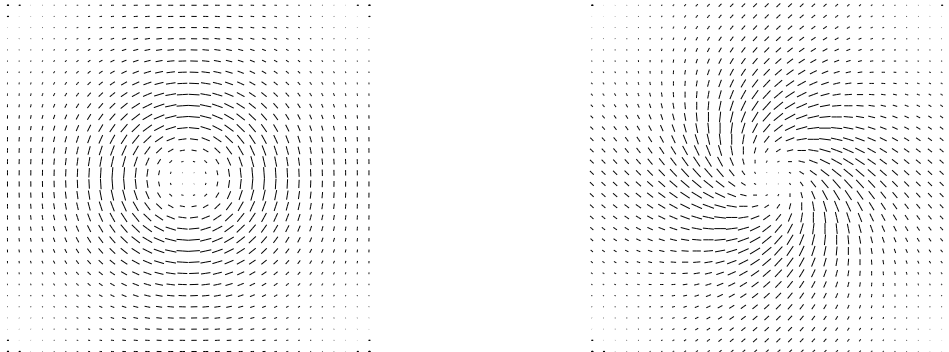


FIG. 1: Gaussian “hot spots.” The left panel is purely E-component, and the right panel is purely B-component.

density perturbations produce only the E component, leaving the B component as a clean probe of subdominant sources of polarization such as tensor perturbations.²

Given a full-sky polarization map, it is possible to separate the E and B components perfectly; with incomplete sky coverage, however, there is inevitably some cross-contamination between the components. This naturally makes detecting the B-component more difficult, as it is in danger of being swamped by the (typically much larger) E-component. In this paper, we will examine the experimental requirements to detect both E and B-component polarization signals in a degree-scale experiment, accounting for this cross-contamination.

One approach to separating E from B is to observe in a circular ring [24, 25, 26]. The separation of components is particularly clean in this case, but a strategy involving a two-dimensional map is likely to be much better for measuring power spectrum amplitudes [27], as many more independent modes at a given scale can be found in the data. Attention has therefore been paid to finding normal modes that minimize the complications due to E-B cross-contamination in a two-dimensional map [27, 28]. In the present paper, we adopt a more straightforward approach: we consider the likelihood function of a polarization map in pixel space and compute the Fisher matrix for the normalizations of both E and B power spectra. Since this “brute-force” approach is based on the likelihood function of the full data, it must be at least as good as (*i.e.*, give as small error bars as) any method based on an expansion in normal modes.

The remainder of this paper is organized as follows. In Section II, we review some properties of polarization maps and illustrate the difficulties in splitting a partial-sky map into E and B components. In Section III, we present the Fisher-matrix formalism we will use to determine the detectability of the two components in a given experiment and also present two simple approximation schemes for determining the detectability. Section IV presents our results, and Section V contains a brief discussion.

II. THE E-B DECOMPOSITION

In this section we describe the nature of the E-B decomposition of a polarization field. This description makes no pretense of completeness; much more information on this subject can be found in the literature. See in particular [29, 30] and references therein.

² In addition to tensors, vector perturbations also produce B-component polarization; however, because vector perturbations decay over time, they are not expected to contribute significantly to the observed polarization, at least in the inflation-inspired models we consider in this paper. In some models (topological-defect models in particular), vector perturbations may be sourced at times close to recombination and may therefore be observable, but we do not consider such models in this paper.

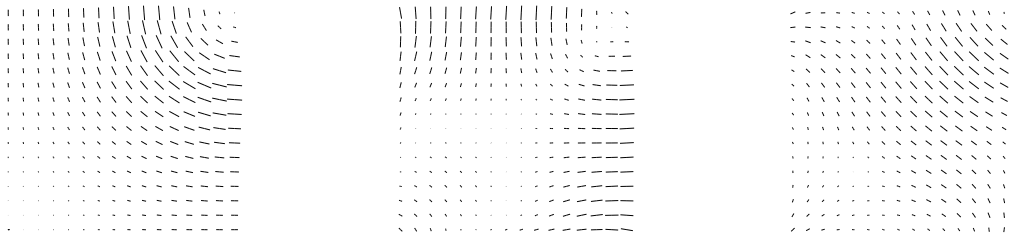


FIG. 2: The left panel is simply one quadrant of the E-component hot spot shown in Figure 1. The center and right panels are a pure E and a pure B component respectively, which sum to equal the left panel.

A. The flat-sky approximation

Polarization is a spin-2 quantity (*i.e.*, it is invariant under 180° rotations). The linear polarization expected to be found in the CMB is described by the two Stokes parameters Q and U , which are related to the magnitude P and direction ϕ of the polarization as follows:

$$Q = P \cos 2\phi, \quad (1)$$

$$U = P \sin 2\phi. \quad (2)$$

There are several ways to describe the division of a polarization map into E and B components. One simple way is to examine a small patch of the sky, which can be well approximated as flat. In this approximation, an E-component polarization field is one whose Stokes parameters satisfy the following equation:

$$2 \frac{\partial^2 Q}{\partial x \partial y} - \left(\frac{\partial^2 U}{\partial x^2} - \frac{\partial^2 U}{\partial y^2} \right) = 0, \quad (\text{E}) \quad (3)$$

while a B-component field satisfies this equation:

$$2 \frac{\partial^2 U}{\partial x \partial y} + \left(\frac{\partial^2 Q}{\partial x^2} - \frac{\partial^2 Q}{\partial y^2} \right) = 0. \quad (\text{B}) \quad (4)$$

(These equations are simply the spin-2 analogues of the equations $\nabla \times \mathbf{v} = 0$ and $\nabla \cdot \mathbf{v} = 0$ for the scalar and pseudoscalar components of a vector field.)

An arbitrary polarization field can always be written as a sum of an E and a B component. One easy way to see this is to work in Fourier space. If we consider a mode with spatial dependence $e^{i\mathbf{k}\cdot\mathbf{x}}$, then equation (3) implies that the E component has a polarization that is always parallel or perpendicular to \mathbf{k} . In terms of the Stokes parameters, it can be written

$$\begin{pmatrix} Q \\ U \end{pmatrix}_E \propto \begin{pmatrix} \cos 2\phi_{\mathbf{k}} \\ \sin 2\phi_{\mathbf{k}} \end{pmatrix} e^{i\mathbf{k}\cdot\mathbf{x}}, \quad (5)$$

where $\phi_{\mathbf{k}}$ is the angle \mathbf{k} makes with the x axis. Similarly, a B-mode has a polarization direction that is always at a 45° angle to \mathbf{k} . It can be obtained by simply rotating the polarization of an E mode through 45° at each point:

$$\begin{pmatrix} Q \\ U \end{pmatrix}_B \propto \begin{pmatrix} -\sin 2\phi_{\mathbf{k}} \\ \cos 2\phi_{\mathbf{k}} \end{pmatrix} e^{i\mathbf{k}\cdot\mathbf{x}}. \quad (6)$$

To decompose an arbitrary map into E and B components, therefore, we simply take the Fourier transforms of Q and U and then, for each wavevector, project (Q, U) onto the axes defined by equations (5) and (6). Of course, to perform this decomposition, we need to know Q and U over all space. If we only know Q and U over a finite region, the Fourier transform and hence the E-B split will depend on the boundary conditions we assume.

Figure 1 shows Gaussian “hot spots” for both the E and B components. Note that the B component, unlike the E component, has handedness; this is the reason that density perturbations, which lack handedness, cannot excite

this component. Of course, we could generate another pair of E, B maps by replacing (Q, U) by $(-Q, -U)$, which is equivalent to rotating the polarizations in these plots through 90° at each point.

To illustrate the ambiguity in the E-B decomposition of an incomplete data set, suppose that we have observed only one quadrant of the E-component hot spot, as shown in the left panel of Figure 2. This is of course a pure E polarization field: it satisfies equation (3) at every point. However, it is also the sum of the E and B polarization fields shown in the center and right panels. These fields were produced by Fourier transforming the region covered by the data with periodic boundary conditions and splitting each Fourier mode into E and B parts according to equations (5) and (6). There are infinitely many other ways the decomposition could have been done; for instance, the data could have been padded with zeroes on all sides before Fourier transforming.

In this particular example, the ‘‘contamination’’ of a pure E component by B is not a small effect: the r.m.s. amplitude of the B component shown in Figure 2 is 0.87 times that of the E component. This is because the map being decomposed has a large amount of power on scales of order the width of the map. In general, we can expect a large amount of cross-contamination between E and B on the largest scales probed by a given data set, with much less contamination on smaller scales. The reason for this is simple: the ambiguity in the E-B decomposition is a result of our ignorance of the boundary conditions to impose on the two components, so the natural length scale associated with E-B mixing is the width of the map.

B. Beyond the flat-sky approximation

Although the flat-sky formulae are in general simpler to work with, for many applications we need to consider the exact, full-sky formulae. In this section we will very briefly summarize this formalism; see [21, 22, 27, 28] for further details and useful identities.

Since polarization is a spin-2 quantity, the natural basis functions to use in expressing the Stokes parameters (Q, U) on the sphere are the spin-2 spherical harmonics. Specifically, we can write

$$Q \pm iU = \sum_{l=2}^{\infty} \sum_{m=-l}^l a_{\mp 2, lm} \mp 2 Y_{lm}, \quad (7)$$

where $\mp 2 Y_{lm}$ is a spin-2 spherical harmonic. Detailed information on the spin-2 spherical harmonics can be found in the sources cited above. For our purposes, all we need to know is that decomposing a polarization field into E and B components is quite simple in the spherical harmonic basis: the coefficients $a_{\mp 2, lm}$ in the expansion can simply be written

$$a_{\pm 2, lm} = E_{lm} \pm iB_{lm}. \quad (8)$$

This, combined with the reality condition $a_{-2, lm}^* = (-1)^m a_{2, l-m}$, allows one to determine E_{lm} and B_{lm} from the spherical harmonic coefficients.

If we assume that the polarization is a realization of a statistically isotropic random process (*i.e.*, that there is no preferred direction), then the ensemble averages $\langle E_{lm} \rangle$ and $\langle B_{lm} \rangle$ must both vanish, and the covariances must satisfy

$$\langle E_{lm} E_{l'm'}^* \rangle = C_l^E \delta_{ll'} \delta_{mm'}, \quad (9)$$

$$\langle B_{lm} B_{l'm'}^* \rangle = C_l^B \delta_{ll'} \delta_{mm'}. \quad (10)$$

If in addition the random process is parity-invariant (lacks handedness), then

$$\langle E_{lm} B_{l'm'}^* \rangle = 0. \quad (11)$$

Furthermore, if the random process is Gaussian, then the two power spectra C_l^E and C_l^B form a complete description of the random process.³ These power spectra are therefore the only thing a Gaussian theoretical model needs to predict about CMB polarization. Fortunately, theoretical models are capable of computing predicted power spectra with great precision and speed [21, 22], for instance using the publicly available CMBFAST software [31].

Of course, actual observations always involve convolving the true polarization field with the telescope beam. As long as the beam is azimuthally symmetric and purely co-polar, this results in a simple replacement of $C_l^{E,B}$ with

³ There is also the cross-correlation between the E component and the temperature anisotropy. We choose to focus exclusively on polarization data in the present paper, though, ignoring temperature data.

$C_l^{E,B} b_l^2$, where b_l is the Legendre transform of the beam pattern. For a Gaussian beam of width σ_{beam} (FWHM = $\sigma_{\text{beam}}\sqrt{8\ln 2}$), we have

$$b_l^2 = \exp(-l(l+1)\sigma_{\text{beam}}^2). \quad (12)$$

Throughout this paper, we will use $C_l^{E,B}$ to denote the beam-smoothed power spectra.

In the next section, we will consider the analysis of data from a hypothetical CMB polarization experiment. The key ingredients in the analysis are the real-space correlations between measurements at different points, $\langle Q(\mathbf{x}_1)Q(\mathbf{x}_2) \rangle$, $\langle U(\mathbf{x}_1)U(\mathbf{x}_2) \rangle$, and $\langle Q(\mathbf{x}_1)U(\mathbf{x}_2) \rangle$, which can be expressed as sums over the power spectra. Specifically, if Q and U are defined with respect to coordinate axes such that the x axis joins the two points, then

$$\langle Q(\mathbf{x}_1)Q(\mathbf{x}_2) \rangle = \sum_l \left(\frac{2l+1}{4\pi} \right) (C_l^E F_{1l}(\mathbf{x}_1 \cdot \mathbf{x}_2) - C_l^B F_{2l}(\mathbf{x}_1 \cdot \mathbf{x}_2)), \quad (13)$$

$$\langle U(\mathbf{x}_1)U(\mathbf{x}_2) \rangle = \sum_l \left(\frac{2l+1}{4\pi} \right) (C_l^B F_{1l}(\mathbf{x}_1 \cdot \mathbf{x}_2) - C_l^E F_{2l}(\mathbf{x}_1 \cdot \mathbf{x}_2)), \quad (14)$$

$$\langle Q(\mathbf{x}_1)U(\mathbf{x}_2) \rangle = 0, \quad (15)$$

where the functions F_{1l} and F_{2l} can be expressed in terms of Legendre functions as

$$F_{1l}(x) = 2 \left(\frac{\left(\frac{l+2}{1-x^2} \right) P_{l-1}^2(x) - \left(\frac{l-4}{1-x^2} + \frac{l(l-1)}{2} \right) P_l^2(x)}{(l-1)l(l+1)(l+2)} \right), \quad (16)$$

$$F_{2l}(x) = 4 \left(\frac{(l+2)P_{l-1}^2(x) - (l-1)xP_l^2(x)}{(l-1)l(l+1)(l+2)(1-x^2)} \right). \quad (17)$$

In practice, we often wish to know the correlations in some other coordinate system. Since we know how (Q, U) transforms under rotations, we can easily get these correlations by applying the appropriate rotation matrices to the correlations given above. (A pleasingly explicit recipe for doing this can be found in [27].)

III. FORMALISM

A. Likelihoods and Fisher Matrices

The Fisher information matrix provides a useful way to quantify the ability of a data set to estimate parameters. It has been applied to great effect in the study of CMB temperature anisotropy (*e.g.*, [32]) and also to CMB polarization studies [27, 33]. In this section, we show how the Fisher matrix can be used to calculate the significance with which the amplitudes of the E and B power spectra can be measured from a polarization map.

Suppose we have made maps containing Q and U measurements at N pixels. The pixel locations are $\mathbf{x}_1, \dots, \mathbf{x}_N$. Our $2N$ data points can be written

$$q_i = Q(\mathbf{x}_i) + \epsilon_{Qi}, \quad (18)$$

$$u_i = U(\mathbf{x}_i) + \epsilon_{Ui}. \quad (19)$$

Here i ranges over pixels in the map, and ϵ_{Qi} (ϵ_{Ui}) is the noise in the i th pixel of the Q (U) map. We will assume uncorrelated noise:

$$\langle \epsilon_{Ai} \epsilon_{Bj} \rangle = \sigma_{Ai}^2 \delta_{AB} \delta_{ij}. \quad (20)$$

Here A and B range over $\{Q, U\}$, and σ_{Ai}^2 is the noise variance in pixel i of map A .

We will arrange our data points into a data vector,

$$\mathbf{d} = \begin{pmatrix} q_1 \\ \vdots \\ q_N \\ u_1 \\ \vdots \\ u_N \end{pmatrix}. \quad (21)$$

The $2N \times 2N$ data covariance matrix is defined to be $\mathbf{M} = \langle \mathbf{d}\mathbf{d}^T \rangle$. We can label elements of the data vector with a pair of indices iA , with i ranging from 1 to N and A being either Q or U . Then a typical element of the covariance matrix is M_{iAjB} . The covariance matrix contains contributions from signal and noise

$$M_{iAjB} = M_{iAjB}^S + M_{iAjB}^N, \quad (22)$$

with

$$M_{iQjQ}^S = w_Q(\mathbf{x}_i, \mathbf{x}_j) \equiv \langle Q(\mathbf{x}_i)Q(\mathbf{x}_j) \rangle, \quad (23)$$

$$M_{iUjU}^S = w_U(\mathbf{x}_i, \mathbf{x}_j) \equiv \langle U(\mathbf{x}_i)U(\mathbf{x}_j) \rangle, \quad (24)$$

$$M_{iQjU}^S = w_X(\mathbf{x}_i, \mathbf{x}_j) \equiv \langle Q(\mathbf{x}_i)U(\mathbf{x}_j) \rangle, \quad (25)$$

$$M_{iAjB}^N = \sigma_{iA}^2 \delta_{ij} \delta_{AB}. \quad (26)$$

As described in the previous section, the correlation functions w_Q, w_U, w_X can be expressed as sums over the power spectra.

A theory predicts a pair of power spectra C_l^E and C_l^B and hence a covariance matrix \mathbf{M} . The likelihood of a theory is

$$\mathcal{L}(\mathbf{M}) \propto (\det \mathbf{M})^{-1/2} \exp\left(-\frac{1}{2} \mathbf{d}^T \mathbf{M}^{-1} \mathbf{d}\right). \quad (27)$$

It is more convenient to work with the quantity

$$L = \ln \det \mathbf{M} + \mathbf{d}^T \mathbf{M}^{-1} \mathbf{d} = -2 \ln \mathcal{L} + \text{const}, \quad (28)$$

which can also be written in the following convenient form:

$$L = \text{Tr}(\ln \mathbf{M} + \mathbf{M}^{-1} \mathbf{d}\mathbf{d}^T). \quad (29)$$

(The logarithm of a matrix is as usual defined via the Taylor series, or equivalently by diagonalizing the matrix and taking the logarithms of its eigenvalues.)

Now suppose that we are considering a class of theories that contains P unknown parameters $\alpha_1 \dots, \alpha_P$, and suppose for simplicity that the covariance matrix is linear in these parameters, so that we can write

$$\mathbf{M} = \mathbf{M}^{(0)} + \sum_{p=1}^P (\alpha_p - 1) \mathbf{M}^{(p)}. \quad (30)$$

Here $\mathbf{M}^{(0)}$ represents the (unknown) true covariance matrix. In other words, the true values of the parameters have been taken to be one. Our ability to measure parameters will be determined by how sharply peaked the likelihood is about its maximum, so we perform a Taylor expansion in L to determine this. If we let ∂_p stand for $\partial/\partial\alpha_p$, then

$$\partial_p L = \text{Tr}(\mathbf{M}^{-1} \partial_p \mathbf{M} - \mathbf{M}^{-1} (\partial_p \mathbf{M}) \mathbf{M}^{-1} \mathbf{d}\mathbf{d}^T) = \text{Tr}(\mathbf{M}^{-1} \mathbf{M}^{(p)} - \mathbf{M}^{-1} \mathbf{M}^{(p)} \mathbf{M}^{-1} \mathbf{d}\mathbf{d}^T). \quad (31)$$

Note that in the ensemble average, $\langle \mathbf{d}\mathbf{d}^T \rangle = \mathbf{M}^{(0)}$, so $\langle \partial_p L \rangle = 0$ when all parameters are equal to one.

The quantity that characterizes the sharpness of the likelihood peak is of course the second derivative, so we must plunge ahead and differentiate again:

$$\partial_q \partial_p L = \text{Tr}\left(-\mathbf{M}^{-1} \mathbf{M}^{(q)} \mathbf{M}^{-1} \mathbf{M}^{(p)} + \mathbf{M}^{-1} \mathbf{M}^{(q)} \mathbf{M}^{-1} \mathbf{M}^{(p)} \mathbf{M}^{-1} \mathbf{d}\mathbf{d}^T + \mathbf{M}^{-1} \mathbf{M}^{(p)} \mathbf{M}^{-1} \mathbf{M}^{(q)} \mathbf{M}^{-1} \mathbf{d}\mathbf{d}^T\right). \quad (32)$$

Let us take an ensemble average of this quantity and evaluate it at $\mathbf{M} = \mathbf{M}^{(0)}$ (which is both the true value and the ensemble-average maximum-likelihood location). Then

$$2F_{qp} \equiv \langle \partial_q \partial_p L |_{\mathbf{M}=\mathbf{M}^{(0)}} \rangle = \text{Tr}\left(\mathbf{M}^{(0)-1} \mathbf{M}^{(q)} \mathbf{M}^{(0)-1} \mathbf{M}^{(p)}\right) \quad (33)$$

The quantities F_{qp} are the elements of the $P \times P$ Fisher matrix \mathbf{F} . They tell us the expected uncertainty with which a parameter α_p can be determined from a likelihood analysis. Specifically, if all parameters except the p th are known *a priori*, then α_p will be determined with an expected error of $1/\sqrt{F_{pp}}$. If on the other hand all parameters are

unknown, then the uncertainty is in α_p is $\sqrt{(\mathbf{F}^{-1})_{pp}}$. Furthermore, these expected uncertainties are the smallest that can be obtained from this data set by any unbiased data analysis method.

We will be interested in determining whether the E- and B-component polarizations can be detected by a given experiment. Let us make an admittedly optimistic assumption: suppose that the *shapes* of the power spectra C_l^E and C_l^B are known but the amplitudes are not. Then we will have two parameters α_E and α_B , such that

$$C_l^{E,B} = \alpha_{E,B} \hat{C}_l^{E,B}, \quad (34)$$

where $\hat{C}_l^{E,B}$ represents the true power spectrum. Then the matrices $\mathbf{M}^{(E)}$ and $\mathbf{M}^{(B)}$ that appear in equation (33) are simply the parts of \mathbf{M} (and in particular \mathbf{M}^S) proportional to C_l^E and C_l^B .

We will say that the E (B) component is detectable if the parameter α_E (α_B) can be measured with an expected uncertainty considerably less than one. Specifically, if α_E has an expected uncertainty of $\frac{1}{q}$, then we can expect to measure the amplitude of C_l^E with a signal-to-noise ratio of q . So if, say, we are interested in knowing whether a particular experimental design will provide a 3-sigma detection of the E component, we simply compute the 2×2 Fisher matrix \mathbf{F} and determine whether $\sqrt{(\mathbf{F}^{-1})_{EE}} > 3$.

B. The JKW Approximation

In the next section, we will present experimental requirements for detecting the E and B components, using the formalism described above. This process is somewhat laborious, since it involves manipulating $2N \times 2N$ matrices, so simpler methods are clearly desirable. One very useful such approximation has been provided by Jaffe, Kamionkowski, & Wang (hereinafter JKW) [33]. Similar results may be found in [25]. In this section, we present a brief heuristic “derivation” of the JKW approximation.

First, consider an experiment in which the N pixels cover the entire sky uniformly. Let us also suppose that the noise level σ^2 is the same in each pixel of the Q and U maps. (In other words, σ^2 is the same as σ_{Ai}^2 of equation (20) and is assumed to be the same across all pixels of both maps.) The analysis of this experiment is quite simple: we can estimate each coefficient $a_{\pm 2,lm}$, and hence each E_{lm} and B_{lm} , independently by exploiting the orthonormality of the spherical harmonics over the whole sphere. Each coefficient will have noise of amplitude

$$\sigma_*^2 = \frac{4\pi}{N} \sigma^2. \quad (35)$$

It is convenient to define the weight w of a set of Q and U maps to be⁴

$$w \equiv \sum_{i=1}^N \sum_{A=\{Q,U\}} \sigma_{Ai}^{-2}. \quad (36)$$

The results of this section depend on the assumption of uniform noise, so $w = 2N/\sigma^2$. Equation (35) can therefore be written

$$\sigma_*^2 = \frac{8\pi}{w}. \quad (37)$$

If we wish to estimate the E-component power spectrum C_l^E , therefore, we have at our disposal a set of independent Gaussian random numbers \hat{E}_{lm} (estimators of the true coefficients E_{lm}) with zero mean and variances

$$\langle |\hat{E}_{lm}|^2 \rangle = C_l^E + \sigma_*^2. \quad (38)$$

Since all the variables are independent, the likelihood has the usual Gaussian form:

$$\mathcal{L} \propto \left(\prod_{l,m} (C_l^E + \sigma_*^2) \right)^{-1/2} \exp \left(-\frac{1}{2} \sum_{l,m} \frac{|E_{lm}|^2}{C_l^E + \sigma_*^2} \right). \quad (39)$$

⁴ Beware: this definition differs by a factor 4π from the weight as defined in JKW. While we’re on the subject, note that the polarization power spectra in JKW and also in Ref. [22] differ by a factor of two from those found elsewhere in the literature and in this paper.

If we assume as before that only the overall normalization of the power spectrum is unknown, we can determine its expected uncertainty just as in the previous section, by computing the Fisher matrix (which is diagonal for a full-sky experiment). Differentiating the above expression for \mathcal{L} twice, we find that the uncertainty in the parameter α_E is given by

$$(SNR)_E^2 \equiv \sigma_{\alpha_E}^{-2} = \frac{1}{2} \sum_{l,m} \left(\frac{C_l^E}{C_l^E + \sigma_*^2} \right)^2 = \frac{1}{2} \sum_{l=2}^{\infty} \frac{2l+1}{(1 + (8\pi/wC_l^E))^2}. \quad (40)$$

Here SNR stands for “signal-to-noise ratio.” An experiment with an SNR of, say, 3, is one in which we would expect to measure the power spectrum normalization with an accuracy of three sigma. Of course, an identical relation applies to α_B .

This result has a very simple interpretation [25]. The quantity $wC_l^E/8\pi$ is the square of the signal-to-noise ratio for a single mode at multipole l . Modes for which this quantity is much greater than unity contribute 1 to the sum, while modes for which it is much less than one contribute nothing. Therefore, what this formula says, roughly, is that the square of the signal-to-noise ratio of the power spectrum amplitude is equal to $\frac{1}{2}$ the number of modes that are detected with high signal-to-noise.

Now consider an experiment that only covers a fraction of the sky f_{sky} . The number of independent modes that can be detected will of course be reduced by a factor f_{sky} . On the other hand, the noise variance for each mode will be reduced by the same factor, since the total weight of the experiment is concentrated in a smaller area. We might guess, therefore, that the generalization of equation (40) to the case of partial sky coverage is

$$(SNR)_{E,B}^2 = \frac{f_{\text{sky}}}{2} \sum_l \frac{2l+1}{(1 + (8\pi f_{\text{sky}}/wC_l^{E,B}))^2}. \quad (41)$$

Equation (41) is the JKW approximation (compare to equation (1) of JKW).

A question arises as to the lower limit of the sum. JKW advocate starting the sum at $l_{\text{min}} = 180^\circ/L$, where L is the survey size, on the grounds that modes with smaller l cannot be probed. It can be argued, though, that the sum should begin at the lowest possible l (namely 2). After all, the fact that modes with low l are not probed is already accounted for by the inclusion of the prefactor f_{sky} . The effective number of independent modes below some multipole l_0 is approximately $f_{\text{sky}} l_0^2$, which is better approximated by $f_{\text{sky}} \sum_2^{l_0} (2l+1)$ than by $f_{\text{sky}} \sum_{l_{\text{min}}}^{l_0} (2l+1)$. The choice made makes little difference to the final results (at most about 20%, and usually much less, for the results to be shown below), so for consistency we follow JKW’s prescription.

Of course, the JKW approximation does not account for the mixing of E and B modes due to incomplete sky coverage. We therefore expect it to overestimate the detectability of the subdominant B component, since some modes that are used to estimate B will be swamped by contamination from the larger E component. As we will see below, this is indeed the case. Perhaps more surprising is the fact that the JKW approximation sometimes *underestimates* the detectability of the E component. In the next subsection, we will consider an enhanced version of the JKW approximation that sheds some light on the reason for this.

C. A toy model of E-B mixing

In this section, we will consider an experiment that covers a square patch of sky that is small enough to permit the use of the flat-sky approximation. Suppose as usual that the sky polarization is a Gaussian random field $\mathbf{p} = \begin{pmatrix} Q \\ U \end{pmatrix}$. It can of course be written as a Fourier transform,

$$\mathbf{p} = \int d^2k \tilde{\mathbf{p}}(\mathbf{k}) e^{i\mathbf{k}\cdot\mathbf{x}}, \quad (42)$$

and each Fourier component can be split into an E and a B part:

$$\tilde{\mathbf{p}}(\mathbf{k}) = \tilde{E}(\mathbf{k}) \begin{pmatrix} \cos 2\phi_{\mathbf{k}} \\ \sin 2\phi_{\mathbf{k}} \end{pmatrix} + \tilde{B}(\mathbf{k}) \begin{pmatrix} -\sin 2\phi_{\mathbf{k}} \\ \cos 2\phi_{\mathbf{k}} \end{pmatrix}. \quad (43)$$

The assumption that the polarization is a realization of a homogeneous, isotropic, parity-invariant Gaussian random field means that \tilde{E} and \tilde{B} are Gaussian random variables with zero mean and covariances

$$\langle \tilde{E}(\mathbf{k}) \tilde{E}^*(\mathbf{k}') \rangle = \frac{1}{(2\pi)^2} C^E(k) \delta(\mathbf{k} - \mathbf{k}'), \quad (44)$$

$$\langle \tilde{B}(\mathbf{k})\tilde{B}^*(\mathbf{k}') \rangle = \frac{1}{(2\pi)^2} C^B(k) \delta(\mathbf{k} - \mathbf{k}'), \quad (45)$$

$$\langle \tilde{E}(\mathbf{k})\tilde{B}^*(\mathbf{k}') \rangle = 0. \quad (46)$$

The power spectra C^E and C^B depend only on the magnitude of \mathbf{k} . The factor of $(2\pi)^2$ is inserted for consistency with standard normalization conventions: $C^{E,B}(k) \approx C_l^{E,B}$ with $l = k$.

Now, suppose that the polarization is measured over a square patch of sky of area L^2 . We might⁵ choose to analyze such a data set by expanding the observed region in a Fourier series with coefficients

$$\tilde{\mathbf{a}}(\mathbf{q}) = \frac{1}{L^2} \int_{L^2} d^2x \mathbf{p}(\mathbf{x}) e^{-i\mathbf{q}\cdot\mathbf{x}}, \quad (47)$$

where $\mathbf{q} = (2\pi/L)(n_x, n_y)$ for integers n_x and n_y .

These Fourier series coefficients are related to the true Fourier transform in the usual way,

$$\tilde{\mathbf{a}}(\mathbf{q}) = \int d^2k \tilde{\mathbf{p}}(\mathbf{k}) W(\mathbf{k} - \mathbf{q}), \quad (48)$$

where the window function is

$$W(\boldsymbol{\gamma}) = \left(\frac{\sin \gamma_x L/2}{\gamma_x L/2} \right) \left(\frac{\sin \gamma_y L/2}{\gamma_y L/2} \right). \quad (49)$$

In other words, each mode $\tilde{\mathbf{a}}(\mathbf{q})$ probes a range of \mathbf{k} values of width $\sim L^{-1}$ around \mathbf{q} .

Suppose that we wish to estimate the E and B power spectra from these Fourier coefficients. We might proceed by decomposing each $\tilde{\mathbf{a}}(\mathbf{q})$ into an ‘‘E’’ and ‘‘B’’ piece:

$$\tilde{\mathbf{a}}(\mathbf{q}) = \tilde{a}_E \begin{pmatrix} \cos 2\phi_{\mathbf{q}} \\ \sin 2\phi_{\mathbf{q}} \end{pmatrix} + \tilde{a}_B \begin{pmatrix} -\sin 2\phi_{\mathbf{q}} \\ \cos 2\phi_{\mathbf{q}} \end{pmatrix} \quad (50)$$

However, since $\tilde{\mathbf{a}}(\mathbf{q})$ contains contributions from a wide range of \mathbf{k} 's, not all of which are parallel to \mathbf{q} , these will not really be purely E or B. In fact, the mean-square value of the supposedly E component is

$$\langle |\tilde{a}_E(\mathbf{q})|^2 \rangle = \frac{1}{(2\pi)^2} \int d^2k (C^E(k) \cos^2 2\alpha + C^B(k) \sin^2 2\alpha) W^2(\mathbf{k} - \mathbf{q}), \quad (51)$$

where $\cos \alpha = \hat{\mathbf{k}} \cdot \hat{\mathbf{q}}$. A similar equation holds for the B component.

When q is large compared to $1/L$, of course, all values of \mathbf{k} that contribute significantly to the integral are quite close in direction to \mathbf{q} , so $\sin^2 2\alpha \approx 0$ and $\tilde{a}_E(\mathbf{q})$ really does depend almost entirely on the E component. In other words, mixing of E and B is relatively unimportant on small scales. But for small \mathbf{q} , α cannot be taken to be small. In fact, if we assume that the power spectra are approximately constant over the range where the window function is large, we can pull them out of the integral to find

$$\langle |\tilde{a}_E(\mathbf{q})|^2 \rangle \approx \frac{1}{L^2} \left(C^E(q) \overline{c_{\mathbf{q}}^2} + C^B(q) \overline{s_{\mathbf{q}}^2} \right), \quad (52)$$

where $\overline{c_{\mathbf{q}}^2}$ and $\overline{s_{\mathbf{q}}^2}$ are the averages of $\cos^2 2\alpha$ and $\sin^2 2\alpha$ weighted by $W^2(\mathbf{k} - \mathbf{q})$. Similarly,

$$\langle |\tilde{a}_B(\mathbf{q})|^2 \rangle \approx \frac{1}{L^2} \left(C^B(q) \overline{c_{\mathbf{q}}^2} + C^E(q) \overline{s_{\mathbf{q}}^2} \right). \quad (53)$$

We can find these averages by numerical integration. Averaging over the direction of \mathbf{q} , we get approximately

$$1 - \overline{c_q^2} = \overline{s_q^2} = \frac{2.4}{qL}. \quad (54)$$

⁵ In fact, we probably would not analyze the data in quite such a naïve way; we would at least taper the edges to reduce ringing in the Fourier modes. But we're trying to keep things simple.

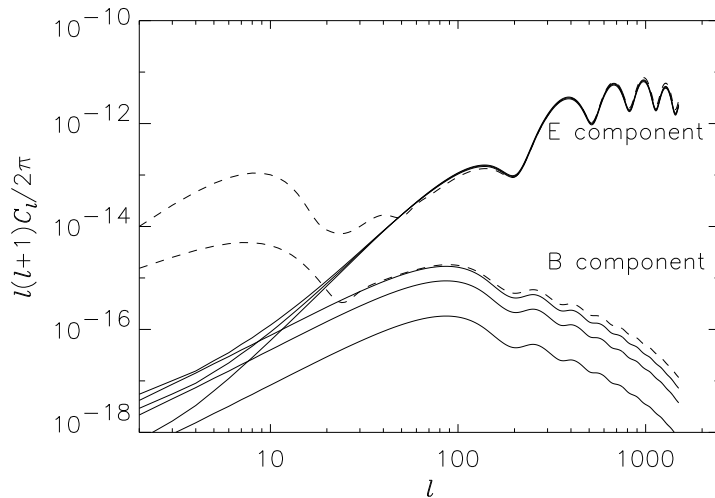


FIG. 3: E and B Power Spectra. The solid curves are the Λ CDM models with no reionization described in the text. From top to bottom, T/S takes the values 0.1, 0.05, 0.01. The dashed curve is a reionized model with $\tau = 0.3$, $T/S = 0.1$, and n tilted to 1.15.

(If we are a bit more sophisticated and taper the edges of the data before Fourier transforming, then the window function W doesn't ring so much, and $\overline{s_q^2}$ can be reduced by ~ 10 -20%. As we will see in the next section, though, this approximation gives surprisingly good results as is.)

Now suppose that $C^E \gg C^B$. Then for each \mathbf{q} with a reasonably large value of $\overline{s_q^2}$ we will have two independent⁶ modes that are dominated by E, rather than the expected one: according to equation (53), even the nominal B mode $\tilde{a}_B(\mathbf{q})$ is mostly E! Since, as we have seen in the previous section, the signal-to-noise ratio is determined by counting the number of modes with high signal-to-noise, this enhances the significance with which α_E can be measured.

In fact, we can modify the JKW approximation to take this into account. Each “nominal E mode” $\tilde{a}_E(\mathbf{q})$ provides a measurement of the E-mode with mean-square amplitude $C_l^E \overline{c_l^2}$ and mean-square noise $8\pi f_{\text{sky}}/w + C_l^B \overline{s_l^2}$. (Here $|\mathbf{q}| = l$. We are imagining an attempt to measure the E-component, so we treat the B-component part of the signal as if it were noise.) We can therefore replace $8\pi f_{\text{sky}}/w C_l^E$ in equation (41) with

$$\kappa_{1l} \equiv \frac{8\pi f_{\text{sky}}/w + C_l^B \overline{s_l^2}}{C_l^E \overline{c_l^2}}. \quad (55)$$

And we should also include a term that accounts for the fact that $\tilde{a}_B(\mathbf{q})$ can be used to measure the E-mode amplitude:

$$\kappa_{2l} \equiv \frac{8\pi f_{\text{sky}}/w + C_l^B \overline{c_l^2}}{C_l^E \overline{s_l^2}}. \quad (56)$$

The final result is

$$(SNR)_E^2 = \frac{f_{\text{sky}}}{2} \sum_l (2l+1) \left(\frac{1}{(1+\kappa_{1l})^2} + \frac{1}{(1+\kappa_{2l})^2} \right). \quad (57)$$

Although this looks quite messy, the interpretation is fairly simple. κ_{1l}^{-1} and κ_{2l}^{-1} are the squared signal-to-noise ratios with which the E-component amplitude can be detected in each mode (counting the B-component contribution as noise). Modes with high signal-to-noise contribute one to the sum, while modes with low signal-to-noise (or low E-signal-to-B-signal, since B-signal is being counted as noise) contribute zero. In the no-mixing limit, $\overline{s_l^2} \rightarrow 0$, the κ_{2l} term doesn't contribute, and the κ_{1l} term agrees with equation (41).

⁶ It can be shown that correlations between the different modes are relatively weak. This is not terribly precise, but after all this section is called “a toy model”!

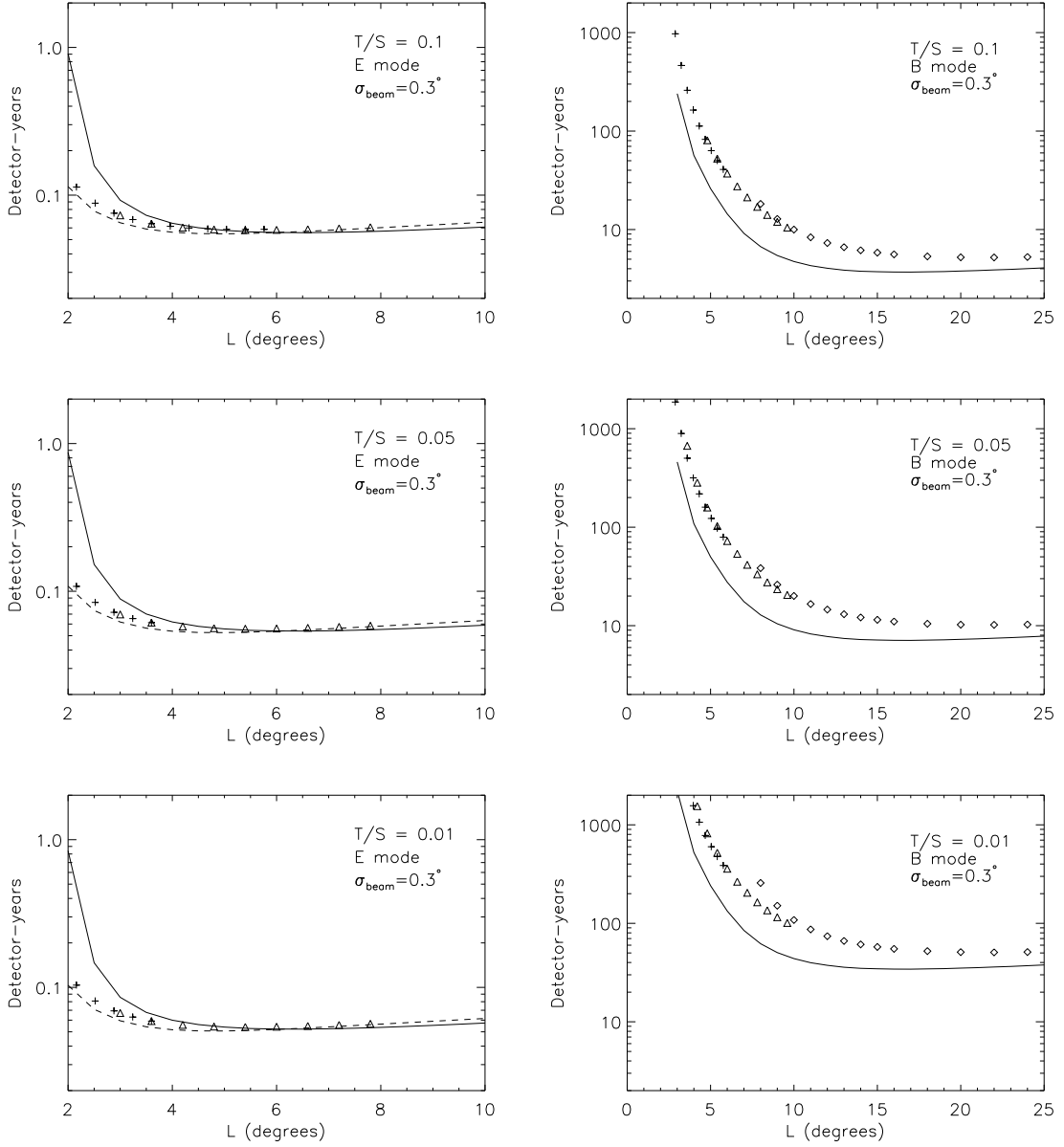


FIG. 4: E and B component detectability for different tensor-scalar ratios. In this figure and the next, the vertical axis is the observing time in detector-years, at a nominal sensitivity of $100 \mu\text{K s}^{1/2}$, required for a 3-sigma measurement of the power spectrum amplitude. The beam size is $\sigma_{\text{beam}} = 0.3^\circ$ (FWHM= 0.71°). The points are the results of the Fisher matrix analysis. The three different symbols are for maps with pixel sizes of 0.18° , 0.3° , and 0.5° . The solid line is the result found with the JKW approximation. In the E-component case, the result of the enhanced JKW approximation is shown as a dashed line.

Incidentally, we now face the same question as in the original JKW approximation regarding the lower limit of the sum. As before, it makes relatively little difference whether we start the sum at 2 or at $180^\circ/L$. In the results shown below, we have started the sum at 2.

We can try to use this approximation to find the B-component detectability, but it turns out to give terrible results. This is not surprising: because we can always measure the E component more accurately than the B component, modeling it simply as an unknown source of noise is a poor approximation.

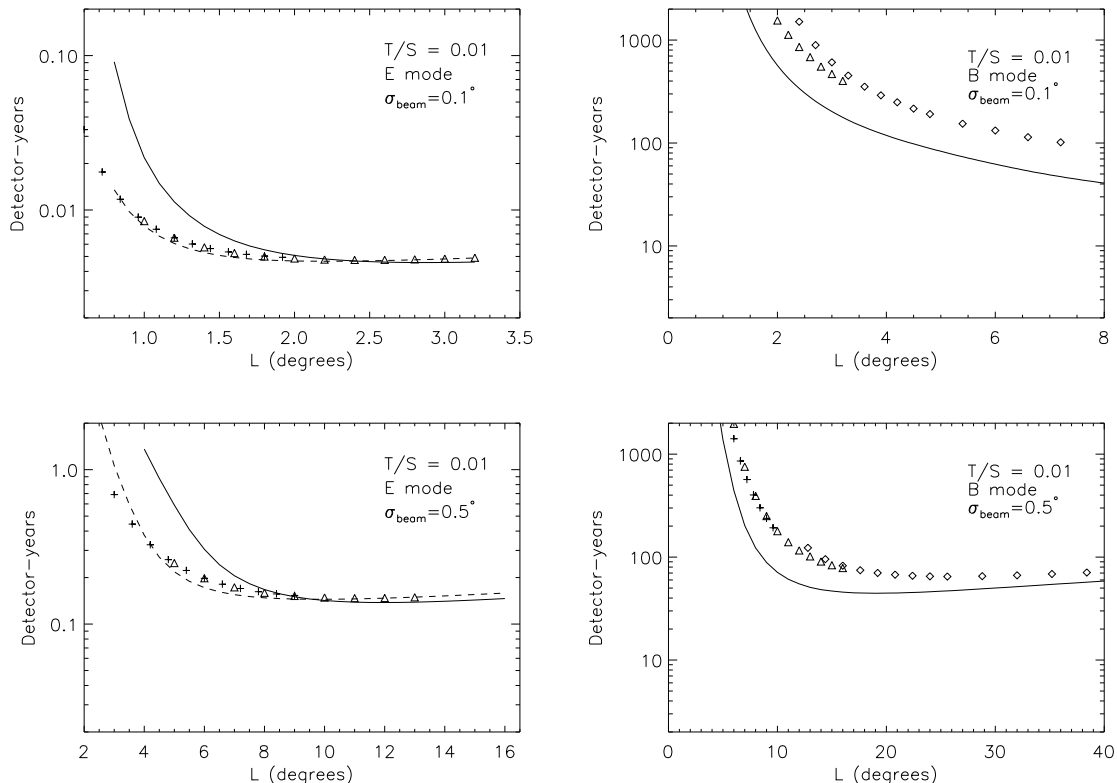


FIG. 5: E and B component detectability for different beam sizes. The results shown here all have $T/S = 0.01$. The symbols have the same meanings as in Figure 4, except for the pixel sizes: for a beam size of 0.1° , the different symbols represent pixel sizes of $0.06^\circ, 0.1^\circ, 0.15^\circ$, while for the 0.5° beam the symbols represent $0.3^\circ, 0.5^\circ, 0.8^\circ$ pixels.

IV. RESULTS

Consider an experiment in which a square patch of sky of length L is observed. We will suppose that the patch is pixelized into an $N_{\text{side}} \times N_{\text{side}}$ square array and that both Q and U are measured in each pixel, so that the dimension of our data vector \mathbf{d} is $2N_{\text{side}}^2$. Suppose furthermore that the noise level σ is the same for all of these measurements. The weight of the experiment is then

$$w = \frac{2N_{\text{side}}^2}{\sigma^2}. \quad (58)$$

The weight is of course proportional to the observing time: $w = N_{\text{d}} t_{\text{obs}} T_0^2 / s^2$, where N_{d} is the number of detectors and t_{obs} is the observing time. $T_0 = 2.728$ K is the current CMB temperature. Its presence is simply to convert units: we choose to measure the sensitivity s in temperature units but the power spectra in dimensionless $\Delta T/T$ units. Instead of quoting weights, therefore, we can simply quote observing times in, say, detector-years at some nominal sensitivity level. In the results below, we will use $s = 100 \mu\text{K s}^{1/2}$ as our nominal sensitivity, so our observing times in detector-years will simply be

$$\text{Detector-years} \equiv N_{\text{d}} \left(\frac{t_{\text{obs}}}{1 \text{ year}} \right) \left(\frac{100 \mu\text{K s}^{1/2}}{s} \right)^2 = \frac{w}{2.35 \times 10^{16}}. \quad (59)$$

We consider a ‘‘concordance’’ Λ CDM cosmological model with parameters chosen for reasonable agreement with the bulk of the available data: $h = 0.70, \Omega_{\text{b}} = 0.041, \Omega_{\Lambda} = 0.7, \Omega_{\text{tot}} = 1, n = 1$. In most of our results, we ignore the effects of reionization by setting the optical depth τ to last scattering equal to zero. We allow the tensor-to-scalar ratio T/S , defined as the ratio of the tensor and scalar temperature power spectra at $l = 2$, to vary. E and B power spectra for these models are shown in Figure 3.

Once all of the above parameters have been specified, we can compute the E and B component power spectra with CMBFAST, COBE-normalize [31, 34], and smooth with a Gaussian beam σ_{beam} . We then use the formalism

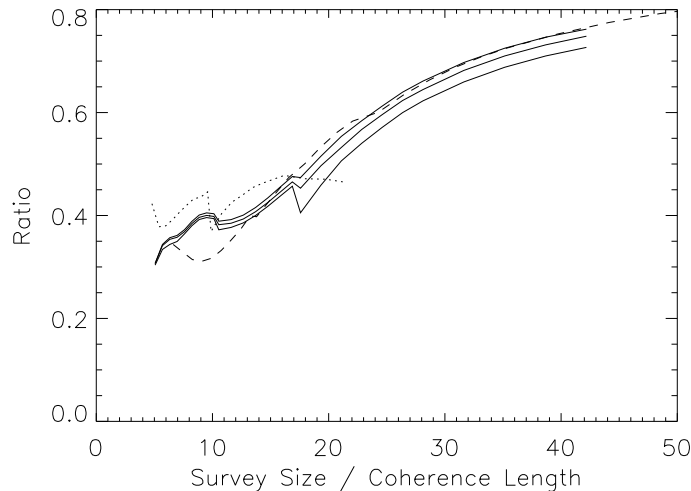


FIG. 6: Comparison of JKW and Fisher matrix detectabilities. The quantity on the vertical axis is the ratio of the required B-mode detection time calculated using the JKW approximation to that calculated from the Fisher matrix. On the horizontal axis is the survey size measured in units of the B-mode coherence length defined in the text. The solid lines are the $\sigma_{\text{beam}} = 0.3^\circ$ models from Figure 4; T/S decreases from top to bottom. The dotted and dashed lines are the 0.1° - and 0.5° -beam models plotted in Figure 5. The kinks in the curves are caused by the fact that different pixel sizes were used in the maps.

of Section III A to calculate the signal-to-noise ratios for the amplitude of the E and B components. Since we are interested in determining the required experimental parameters for a strong detection of the two amplitudes, we fix the desired signal-to-noise at 3 and solve numerically for the required weights. The results are shown in Figures 4 and 5. For comparison, we also show the result of the JKW approximation and, for the case of the E component, the result of the “enhanced” JKW approximation of equation (57). Although most of our results were calculated with $\sigma_{\text{beam}} = 0.3^\circ$, we calculated the $T/S = 0.01$ power spectra for $\sigma_{\text{beam}} = 0.1^\circ$ and 0.5° as well to illustrate the effect of beam size on our results.

In the Fisher matrix analysis, we analyze maps with several different pixel sizes, as indicated in the figure captions. For the 0.3° beam, for example, the largest pixel size is 0.5° , which is somewhat larger than one would ideally like to use. We use this large pixel size so that we can investigate data sets with large sky coverage without having to invert inconveniently large matrices. As shown in the figures, there is overlap in map size between different pixel sizes, which gives a crude idea of the amount of information being lost when large pixel sizes are used. In general, the bulk of the information is found on scales larger than the pixel scale; for maps with a reasonable number of pixels, the fact that we are undersampling the beam does not appear to affect the results very much.

Note that the JKW approximation underestimates the difficulty of detecting the B component as expected. For small survey sizes, though, it overestimates the difficulty of measuring the E component amplitude. The enhanced JKW approximation provides a better fit in this regime.

The detectability of the E component is quite flat as a function of survey size even for fairly small maps, but that of the B component is not. For the case of a 0.3° beam, the optimal survey size for detecting the B component is 22° , as compared to 17° found via the JKW approximation. For $\sigma_{\text{beam}} = 0.5^\circ$, the optimum is 26° , while the JKW approximation would give 19° . For the $\sigma_{\text{beam}} = 0.1^\circ$ case, the optimum survey size was too large to find with the Fisher-matrix formalism. The JKW optimum for this case occurs at $L = 15^\circ$, with a detection time of 30 detector-years; it is reasonable to suppose that the true optimum is at even larger scales.

While it may not be necessary for an experiment to achieve the optimum survey size, one would certainly like to stay well to the right of the “knee” in Figures 4 and 5. For the case of a 0.3° beam, the required detection time is relatively flat for $L \gtrsim 12^\circ$ but rises sharply at smaller L . This suggests that a map of at least 40×40 σ_{beam} -sized pixels should be made in order to measure the B-component amplitude in such an experiment. The experimental weight required for a 3-sigma B-component detection in such an experiment would be such that the B-component-signal-to-noise per pixel is approximately unity.

In order to determine whether reionization made a significant difference to our results, we examined a model in which the optical depth to last scattering was $\tau = 0.3$. In order to keep the temperature power spectrum more or less the same, we tilted the spectral index n from 1 to 1.15. As shown in Figure 3, this makes a large difference to the polarization power spectra, but most of the difference is on larger scales than those to which our degree-scale

experiments are most sensitive. The required detection times for this model were very similar to those in the no-reionization case: for the E-component, the difference was less than 4%, while for the B-component it ranged from 15% down to 5% over the range of survey sizes shown in Figure 4.

V. DISCUSSION

As we have seen in the previous section, the Fisher-matrix formalism gives a slightly better detectability for the E-component power spectrum amplitude than is predicted by the no-mixing JKW approximation, at least in the case of small survey sizes. The reason for this is that some modes that “should” probe the B component are actually dominated by the E component, increasing the number of independent modes that can be used to estimate the E-component amplitude. The enhanced JKW approximation (57) does surprisingly well at characterizing the E-component detectability, confirming that this “extra mode” explanation is indeed correct.

The main practical consequence of the enhanced E-component detectability is that experiment designers need not be terribly concerned about ensuring large sky coverage: the detection requirements are fairly flat as a function of survey size. For the B component, on the other hand, survey size is quite important. The required observation time rises sharply as the survey size decreases. For a 0.3° beam, the “knee” in detectability occurs at a survey size of about 12° .

As expected, the neglect of mixing in the JKW approximation causes it to underestimate the difficulty of measuring the B component. We might expect this underestimation to depend primarily on the survey size, measured relative to some sort of coherence length of the signal being looked for. In Figure 6, we illustrate this by plotting the ratio of the detection time calculated using the JKW approximation to the Fisher-matrix calculation. On the horizontal axis is plotted the survey size, measured in units of the B-component coherence length. The coherence length is defined by $\theta_{\text{coh}} = \pi/l_{\text{coh}}$, where the coherence multipole is

$$l_{\text{coh}} \equiv \frac{\sum_l (2l+1) l^2 C_l^B}{\sum_l (2l+1) l C_l^B}, \quad (60)$$

the weighted average multipole, with weights given by $l(2l+1)C_l^B$. (Here C_l^B is the beam-smoothed power spectrum as usual.) All of the models discussed in the last section are plotted here. In general, the JKW approximation becomes good when the survey size is many coherence lengths, but for $L \lesssim 20$ coherence lengths, it underestimates the detection difficulty by a factor of ~ 2.5 .

It is important to note that the Fisher-matrix formalism used in this paper gives the *best* possible error bars that can be achieved from a given experiment. Even if, for example, we expand the data set in some set of normal modes that minimize E-B mixing [26, 27, 28], we cannot do any better than the brute-force likelihood analysis of the entire data set on which the Fisher-matrix formalism is based. This is not to say, of course, that such methods are not useful. They may reduce computation time, provide insight into the nature of the E-B decomposition, and allow filtered real-space maps of the E and B components to be made, for example.

Although the Fisher-matrix results represent the idealized minimum possible error bars, they are likely to be quite close to the errors achievable in real experiments.⁷ After all, lossless or nearly lossless methods such as those that have been applied to recent temperature anisotropy measurements [1, 2] can be easily adapted to the polarization case. The other idealization that has been made in this analysis is that only the amplitudes, and not the shapes, of the power spectra are unknown. This will of course not be true in a real experiment (although, as long as CMB temperature anisotropy experiments continue to return results consistent with standard models, strong constraints on the shapes will be available); however, for the first few experiments to detect the E and B modes, a band-power estimate of the power spectrum in a few bands will probably be sufficient and may be expected to yield error bars similar in size to those calculated by the Fisher-matrix formalism.

E-B mixing is significant only on scales comparable to the size of the survey, and therefore affects a relatively small number of modes [27, 28]. It might therefore be surprising that mixing has as large an effect on the B-component detectability as it does. The main point to remember in this regard is that the modes with wavelengths of order the survey size are always the ones that are detected with the highest signal-to-noise. (After all, the beam-smoothed C_l^B is invariably a sharply decreasing function of l , whereas the noise has a flat power spectrum.) The loss of these modes to mixing therefore has a disproportionately large effect.

⁷ Unless foreground contamination, which is not treated in the present work, proves to be a serious problem.

It should be noted that the criterion adopted for “detectability” of a component in this paper is that the amplitude of that component’s power spectrum can be measured with small fractional uncertainty. It is possible for a component to be “detected” (*i.e.*, for the null hypothesis that the component is absent to be ruled out) at high significance even if this criterion is not met. For instance, if a single mode is detected with high signal-to-noise, and if that mode is known to be a pure B-mode, with no E-component contamination, then the B-component will have been detected with high significance. However, based on a single mode, the amplitude of the power spectrum cannot be determined with fractional uncertainty less than $O(1)$, so such an experiment would not meet the detectability criterion considered in this paper.

This scenario could easily occur in an experiment designed to measure the Stokes parameters in a thin ring [24, 25, 26]. Because an accurate characterization of the power spectrum amplitudes will be extremely important in interpreting polarization results, and because a detection of the polarization in many different modes is much more robust than a detection in only a few, we have chosen to adopt the stronger detectability criterion of this paper.

The formalism described in this paper has numerous applications. Although we have considered only square maps, it can of course be used to explore the effects of survey geometry on detectability of the two components. It can also easily be adapted to examine the degree to which inhomogeneous noise alters detectability. One might suppose, for instance, that measuring the edges of the survey with high precision would help in separating the two components, since the modes that are “ambiguous” with respect to the E-B split tend to be supported most strongly near the boundary [28]. Finally, the formalism described herein may prove useful in studies of weak gravitational lensing (*e.g.*, [35, 36]): the shear induced by lensing is a spin-2 field, and the mathematics is therefore quite closely analogous to the case of CMB polarization.

Acknowledgments

The author wishes to thank Max Tegmark for useful conversations. This research was begun while the author was an ITP Scholar at the Institute for Theoretical Physics at U.C. Santa Barbara and has been supported in part by NSF grant AST-0098048.

-
- [1] C.B. Netterfield, P.A.R. Ade, J.J. Bock, J.R. Bond, J. Borrill, A. Boscaleri, K. Coble, C.R. Contaldi, B.P. Crill, P. de Bernardis, P. Farese, K. Ganga, M. Giacometti, E. Hivon, V.V. Hristov, A. Iacoangeli, A.H. Jaffe, W.C. Jones, A.E. Lange, L. Martinis, S. Masi, P. Mason, P.D. Mauskopf, A. Melchiorri, T. Montroy, E. Pascale, F. Piacentini, D. Pogosyan, F. Pongetti, S. Prunet, G. Romeo, J.E. Ruhl, and F. Scaramuzzi, *astro-ph/0104460* (2001).
 - [2] A.T. Lee, P. Ade, A. Balbi, J. Bock, J. Borrill, A. Boscaleri, P. de Bernardis, P.G. Ferreira, S. Hanany, V.V. Hristov, A.H. Jaffe, P.D. Mauskopf, C.B. Netterfield, E. Pascale, B. Rabii, P.L. Richards, G.F. Smoot, R. Stompor, C.D. Winant, and J.H.P. Wu, *astro-ph/0104459* (2001).
 - [3] N.W. Halverson, E.M. Leitch, C. Pryke, J. Kovac, J.E. Carlstrom, W.L. Holzapfel, M. Dragovan, J.K. Cartwright, B.S. Mason, S. Padin, T.J. Pearson, M.C. Shepherd, and A.C.S. Readhead, *astro-ph/0104489* (2001).
 - [4] R. Stompor, M. Abroe, P. Ade, A. Balbi, D. Barbosa, J. Bock, J. Borrill, A. Boscaleri, P. De Bernardis, P.G. Ferreira, S. Hanany, V. Hristov, A.H. Jaffe, A.T. Lee, E. Pascale, B. Rabii, P.L. Richards, G.F. Smoot, C.D. Winant, and J.H.P. Wu, *astro-ph/0105062* (2001).
 - [5] J.R. Bond, P. Ade, A. Balbi, J. Bock, J. Borrill, A. Boscaleri, K. Coble, B. Crill, P. de Bernardis, P. Farese, P. Ferreira, K. Ganga, M. Giacometti, S. Hanany, E. Hivon, V. Hristov, A. Iacoangeli, A. Jaffe, A. Lange, A. Lee, L. Martinis, S. Masi, P. Mauskopf, A. Melchiorri, T. Montroy, B. Netterfield, S. Oh, E. Pascale, F. Piacentini, D. Pogosyan, S. Prunet, B. Rabii, S. Rao, P. Richards, G. Romeo, J. Ruhl, F. Scaramuzzi, D. Sforna, K. Sigurdson, G. Smoot, R. Stompor, C. Winant, and P. Wu, *astro-ph/0011378* (2000).
 - [6] A.H. Jaffe, P.A.R. Ade, A. Balbi, J.J. Bock, J.R. Bond, J. Borrill, A. Boscaleri, K. Coble, B.P. Crill, P. de Bernardis, P. Farese, P.G. Ferreira, K. Ganga, M. Giacometti, S. Hanany, E. Hivon, V.V. Hristov, A. Iacoangeli, A.E. Lange, A.T. Lee, L. Martinis, S. Masi, P.D. Mauskopf, A. Melchiorri, T. Montroy, C.B. Netterfield, S. Oh, E. Pascale, F. Piacentini, D. Pogosyan, S. Prunet, B. Rabii, S. Rao, P.L. Richards, G. Romeo, J.E. Ruhl, F. Scaramuzzi, D. Sforna, G.F. Smoot, R. Stompor, C.D. Winant, and J.H.P. Wu, *Phys. Rev. Lett.* **86**, 3475 (2000).
 - [7] M. Tegmark and M. Zaldarriaga, *Phys. Rev. Lett.* **85**, 2240 (2000).
 - [8] <http://map.gsfc.nasa.gov/>
 - [9] <http://astro.estec.esa.nl/SA-general/Projects/Planck/>
 - [10] G. Jungman, M. Kamionkowski, A. Kosowsky, and D.N. Spergel, *Phys. Rev. D* **54**, 1332 (1996)
 - [11] J.R. Bond, G. Efstathiou, and M. Tegmark, *Mon. Not. R. Astron. Soc.* **291**, L33-L41 (1997).
 - [12] S.T. Staggs, J.O. Gundersen, and S. E. Church, in *Microwave Foregrounds*, edited by A. de Oliveira-Costa and M. Tegmark (ASP Conference Series, vol. 181, San Francisco), p. 299.
 - [13] M.M. Hedman, D. Barkats, J.O. Gundersen, S.T. Staggs, and B. Winstein, *Astrophys. J. Lett.* **548**, L111 (2001).

- [14] J.B. Peterson, J.E. Carlstrom, E.S. Cheng, M. Kamionkowski, A.E. Lange, M. Seiffert, D.N. Spergel, and A. Stebbins, astro-ph/9907276 (1999).
- [15] M.J. Rees, *Astrophys. J. Lett.* **153**, L1 (1968).
- [16] A. Kosowsky, *Ann. Phys.* **246**, 49 (1996).
- [17] M. Zaldarriaga, D.N. Spergel, and U. Seljak, *Astrophys. J.* **488**, 1 (1997).
- [18] D.J. Eisenstein, W. Hu, and M. Tegmark, *Astrophys. J.* **518**, 2 (1999).
- [19] M. Bucher, K. Moodley, and N. Turok, astro-ph/0012141 (2001).
- [20] W.H. Kinney, *Phys. Rev. D* **58**, 123506 (1998).
- [21] M. Zaldarriaga and U. Seljak, *Phys. Rev. D* **55**, 1830.
- [22] M. Kamionkowski, A. Kosowsky, and A. Stebbins, *Phys. Rev. D* **55**, 7368 (1997).
- [23] W. Hu, U. Seljak, M. White, and M. Zaldarriaga, *Phys. Rev. D* **57**, 3290 (1998).
- [24] B. Keating, P. Timbie, A. Polnarev, and J. Steinberger, *Astrophys. J.* **495**, 580 (1998).
- [25] M. Zaldarriaga, *Astrophys. J.* **503**, 1 (1998).
- [26] T. Chiueh and C.-J. Ma, astro-ph/0101205 (2001).
- [27] M. Tegmark and A. de Oliveira-Costa, *Phys. Rev. D*, **64**, 063001 (2001).
- [28] A. Lewis, A. Challinor, and N. Turok, astro-ph/0106536 (2001).
- [29] M. Zaldarriaga, *Phys. Rev. D* **64**, 103001 (2001).
- [30] W. Hu & M. White, *New Astronomy* **2**, 323 (1997).
- [31] <http://physics.nyu.edu/matiasz/CMBFAST/cmbfast.html>
- [32] M. Tegmark, A. Taylor, and A. Heavens, *Astrophys. J.* **480**, 22 (1997).
- [33] A.H. Jaffe, M. Kamionkowski, and L. Wang, *Phys. Rev. D* **61**, 083501 (2000) (JKW).
- [34] E.F. Bunn and M. White, *Astrophys. J.* **480**, 6 (1997).
- [35] N. Kaiser, *Astrophys. J.* **498**, 26 (1998).
- [36] W. Hu and M. White, *Astrophys. J.* **554**, 67 (2001).